/

Article / Book Information

Title	Giant nonlinear conductivity in an organic conductor with a sharp metal-insulator transition: beta''-(BEDT-TTF)_3_(HSO_4_)_2_
Authors	Tatsuhiko Ozawa,Kozo Tamura,Yoshimasa Bando,Tadashi Kawamoto,Takehiko Mori,Ichiro Terasaki
Citation	Phys. Rev. B, Vol. 80, No. 15,
/Pub. date	2009, 10
URL/Journal URL	http://journals.aps.org/prb/
/Copyright	Copyright (c) 2009 American Physical Society

Giant nonlinear conductivity in an organic conductor with a sharp metal-insulator transition: β''-(BEDT-TTF)$_3$(HSO$_4$)$_2$

Tatsuhiko Ozawa and Kozo Tamura

Department of Chemistry and Materials Science, Tokyo Institute of Technology, O-okayama, Tokyo 152-8552, Japan

Yoshimasa Bando, Tadashi Kawamoto, and Takehiko Mori

Department of Organic and Polymeric Materials, Tokyo Institute of Technology, O-okayama, Tokyo 152-8552, Japan

Ichiro Terasaki

Department of Applied Physics, Waseda University, Tokyo 169-8555, Japan

The title organic conductor, where BEDT-TTF is bis(ethylenedithio)tetrathia-fulvalene, undergoes a sharp metal-insulator transition at $T_{MI} = 126$ K, below which giant nonlinear conductivity accompanied by negative differential resistance (NDR) is observed. In the usual organic conductors, resistance in the high-current region decreases following the power of current, but the present system shows abrupt NDR. The extraordinary NDR is quantitatively explained by phenomenology based on the energy balance and attributed to the sharp phase transition at T_{MI}. This type of nonlinear transport is called "transition" type in contrast to the conventional "activation" type. The transition type is also characterized by the negative temperature dependence of the threshold power. It is predicted that there is a possibility that oscillating voltage emerges, but chaotic output never appears in this type. The different shapes of the two-probe current-voltage characteristics and pulse responses are also interpreted in view of the small ratio of the low-conducting and high-conducting states.

I. INTRODUCTION

Nonlinear conductivity has been investigated in a number of one-dimensional conductors,[1] but recently nonlinear phenomena in two-dimensional charge order states in manganites and organic conductors have been attracting attention.[2–7] In the organic charge-transfer salt, θ-(BEDT-TTF)$_2$CsCo(SCN)$_4$, spontaneous current oscillation, called an organic thyristor, has been found,[8] and it has been followed by other organic conductors.[9] Although dynamical properties of one-dimensional systems have been extensively investigated starting from the equation of motion of density waves,[1] nonlinear properties in two-dimensional systems are different in many respects. Recently, we have attempted to explain current-voltage characteristics and other related properties starting from the phenomenology based on energy balance,[10] which is mathematically equivalent to the classical thermal dissipation.[11] Previously, we have investigated a system in which the resistivity is expressed in an activated manner in the whole temperature region. The universally observed power-law current-voltage characteristics,[12]

$$\sigma(J,T) = \sigma_1 \exp\left(-\frac{T_a}{T}\right) + \sigma_2 J^m, \qquad (1)$$

is satisfactorily reproduced in this model. Here, the first term represents the conventional ohmic conductivity with activation energy T_a, and the second term represents nonlinear conductivity following the power of current density J. The present paper demonstrates entirely different current-voltage characteristics appear when the system exhibits a sharp phase transition at T_{MI}. We have investigated β''-(BEDT-TTF)$_3$(HSO$_4$)$_2$,[13–15] which undergoes a steep M-I

transition at 126 K as shown in Fig. 1. This compound has a so-called β'' structure, and the ground state is a nonmagnetic charge-order state.[16] In contrast to the previous activation type, we shall call the present case transition type. The transition type is the case where the order parameter vanishes above a certain transition temperature, whereas the activation type corresponds to the simple two-band model where the energy gap is constant. The nonlinear conductivity of these organic charge-transfer compounds is related to the charge-order ground states. The present transition type appears when the low-temperature charge order disappears, and the high-temperature entirely uniform metallic state appears above the abrupt (probably) first-order metal-insulator transition.

II. ENERGY-BALANCE MODEL

High electric fields are expected to modify the Fermi distribution of carriers in conductors.[17] In a semiconductor with
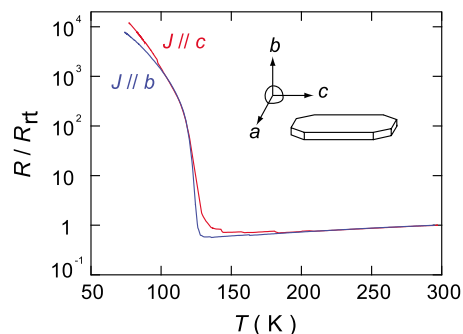

FIG. 1. (Color online) Temperature dependence of in-plane ($\|c$) and out-of-plane ($\|b$) resistivities of β''-(BEDT-TTF)$_3$(HSO$_4$)$_2$. The room-temperature resistivities are 0.028 Ω cm along c and 8.26 Ω cm along b.
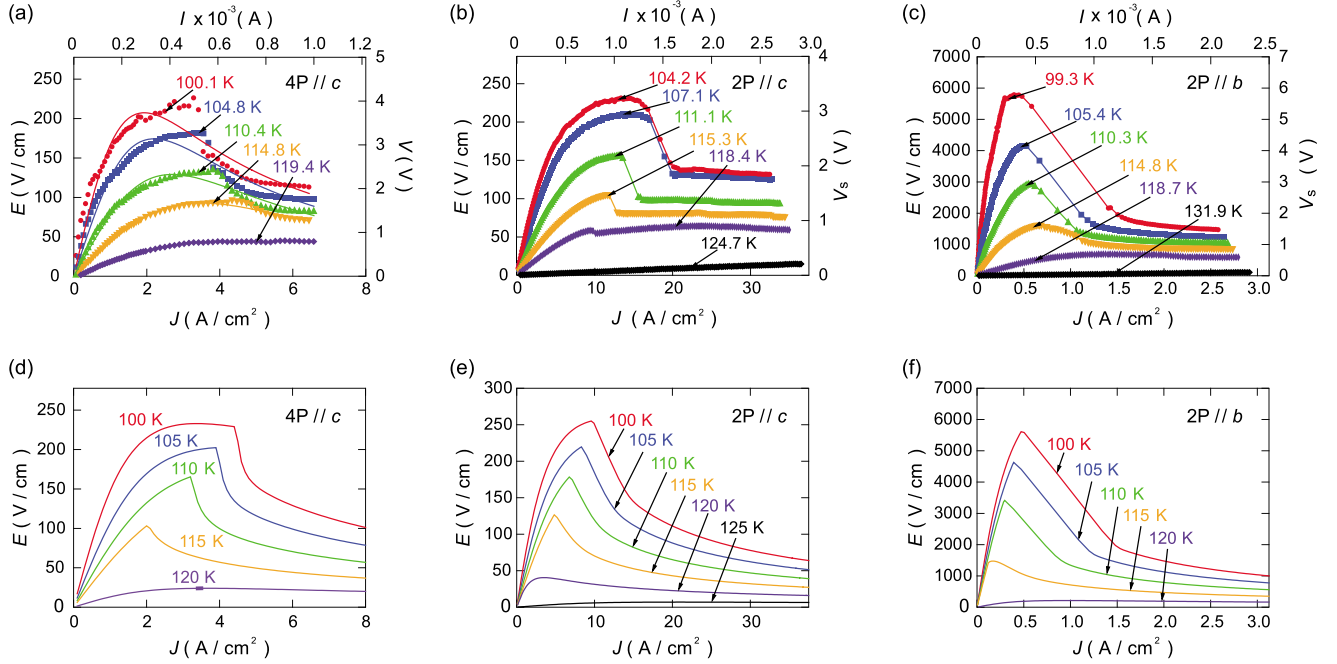
FIG. 2. (Color online) Observed (a)–(c) and simulated (d)–(f) nonlinear conductivity in β''-(BEDT-TTF)$_3$(HSO$_4$)$_2$. (a) J-E characteristics measured by the four-probe method, applying a 5 ms current pulse in the conducting plane ($\|c$). The fitting curves are derived from Eq. (1). (b) J-E characteristics measured by the two-probe method with application of a 5 ms voltage pulse in the conducting plane ($\|c$). (c) J-E characteristics perpendicular to the conducting sheet ($\|b$) measured by the two-probe method. (d) In-plane four-probe J-E characteristics simulated from Eq. (3) so as to reproduce (a). (e) In-plane two-probe measurements ($\|c$). (f) Out-of-plane two-probe measurements ($\|b$).

an energy gap, the equilibrium distribution is reduced to the classical Boltzmann distribution, and what is important is the excited carrier number n_c at the bottom of the conduction band. The conductivity is represented as $\sigma(T) = e n_c \mu$, where e is the elementary electric charge and μ is the mobility of carriers. The temperature dependence of σ mainly comes form n_c (Appendix). Since the conductivity at low fields is represented by a definite function of $\sigma(T)$, we can assume one-to-one correspondence between n_c and the "electron temperature" T_e even at high fields although so-defined T_e may be higher than the real lattice temperature. The electron temperature follows the energy dissipation relation,

$$nC\frac{dT_e}{dt} = P + \nabla(K \nabla T_e), \qquad (2)$$

where nC is the electron heat capacity per volume (C term), $P = J^2/\sigma(T_e)$ represents the supplied energy (P term), and K is the thermal conductivity (K term).[10,11] It should be emphasized that although we are dealing with electron temperature, we do not imagine the sample to be actually heated, but we intend to manipulate the carrier numbers at the excited state (Appendix). In inorganic thin films, such a model leads to spatial distribution of T_e, resulting in filamentary current, whereas organic elongated crystals maintain approximately homogeneous current as experimentally verified by the absence of hysteresis. When T_e is constant everywhere in the sample, the K term is simplified to the Newtonian cooling by using the energy-transfer rate α,

$$nC\frac{dT_e}{dt} = J^2/\sigma(T_e) - \alpha(T_e - T). \qquad (3)$$

This equation is iteratively evaluated at discrete times; the left-hand side affords the change in T_e, and new T_e is introduced in the right-hand side, and the calculation is iterated to give successive change in T_e. The results satisfactorily reproduce the observed current-voltage characteristics and the temperature dependence of the threshold field and current.[10] This difference equation defines nonlinear dynamics with respect to T_e, giving rise to oscillating and chaotic outputs. Previously, we have investigated a system with a temperature-independent energy gap. The present paper describes how the temperature-dependent gap, which is represented by a sharp phase transition in $\sigma(T)$, changes the nonlinear characteristics.

III. EXPERIMENTAL

Black platelike crystals of typical dimensions of 0.80 $\times 0.50 \times 0.02$ mm^3 were obtained by electrochemical crystallization applying a constant current of 0.5 μA for two weeks to a BEDT-TTF solution of 1,1,2-tricholoroethane containing [(C$_4$H$_9$)$_4$N][HSO$_4$] as the supporting electrolyte.[15] Nonlinear conductivity was measured with a short voltage or current pulse of 5 ms length and 1 s interval in order to avoid heating. Nonlinearity was observed when the electric fields were applied along the c and b axes. The sample cross section is $S = 1.52 \times 10^{-4}$ cm^2, and the distance between the voltage contacts is $L = 0.018$ cm for Fig. 2(a), $S = 8.0 \times 10^{-5}$ cm^2 and $L = 0.014$ cm for Fig. 2(b), and S

$=8.0\times10^{-4}$ cm^2 and $L=0.001$ cm for Fig. 2(c). In the simulation, Eq. (3) was calculated in 0.1 ms intervals, and 50 iterations were carried out in order to reproduce a 5 ms pulse. Two adjusting parameters nC and α were chosen so as to reproduce the observed characteristics.

IV. RESULTS

A. Nonlinear characteristics

Figure 2 compares observed and simulated nonlinear characteristics, plotted with respect to the current density J and the electric field E. In the four-probe (4P) measurements, a regulated current pulse is applied to the outer two terminals, and voltage between the inner two terminals is measured [Fig. 2(a)]. NDR is observed below 115 K. The NDR is most clearly observed around 100 K and gradually approaches ohmic when the temperature approaches to T_{MI}. The J-E characteristics are usually well fitted by the power-law phenomenological equation,[17] The fitting curves based on Eq. (1) are depicted in Fig. 2(a). It is obvious that the agreement is not very good; the experimental data exhibit a steep drop in the NDR region. Accordingly, the observed results do not follow the power-law dependence [Eq. (1)].

In the two-probe (2P) measurement, a voltage pulse of V_0 is applied to the circuit, and the sample electric field $E=V_s/L$ is estimated from the sample voltage $V_s=V_0-R_LI$, where $R_L=5$ kΩ is the series load resistance and I is the measured current. Figures 2(b) and 2(c) show the results of such 2P measurements in the in-plane ($\|c$) and out-of-plane ($\|b$) directions, respectively. The J-E characteristics show remarkable NDR. In contrast to inorganic thin films,[11] no hysteresis or switching effects have been observed when V_0 is decreased.

In order to simulate the nonlinear characteristics, $\sigma(T)$ is approximated by a function $\sigma(T)=\sigma_0 \exp(-T_a/T)$ as shown in Fig. 3(a). In the high-temperature region 1, $\sigma(T)$ is almost temperature independent, while the low-temperature region 3 is a slowly varying function. In the intermediate region 2, very sharp change is assumed. By using this model $\sigma(T)$, Eq. (3) is iteratively calculated. Figures 2(d)–2(f) show the calculated characteristics. The 4P characteristics reproduce the sharp NDR region. The calculated 2P characteristics [Figs. 2(e) and 2(f)] reproduce the rounded peak and the jumps sufficiently. The parameters are $nC=0.3$ J/K cm^3 and $\alpha=40$ W/K cm^3 for 4P, whereas α is changed to 100 W/K cm^3 for 2P$\|c$ and 150 W/K cm^3 for 2P$\|b$. These parameters are basically in the same order as the previous compound ($nC=0.1$ J/K cm^3 and $\alpha=200$ W/K cm^3).[10]

In the 2P measurements, the previous system has exhibited a large jump from the low-conducting state to the high-conducting state so that the J-E characteristics are triangular. By contrast, the present system shows a rounded peak at low fields, followed by a comparatively small jump going to the high-conducting state [Figs. 2(b) and 2(c)]. In the previous compound, the low-conducting state has shown as high resistance as 200 kΩ, which jumps to the high conducting state with typically 200 Ω resistance. The present system shows comparatively low resistance, 8 kΩ for $\|c$ and 25 kΩ for $\|b$ in the low-field states at low temperatures. Although
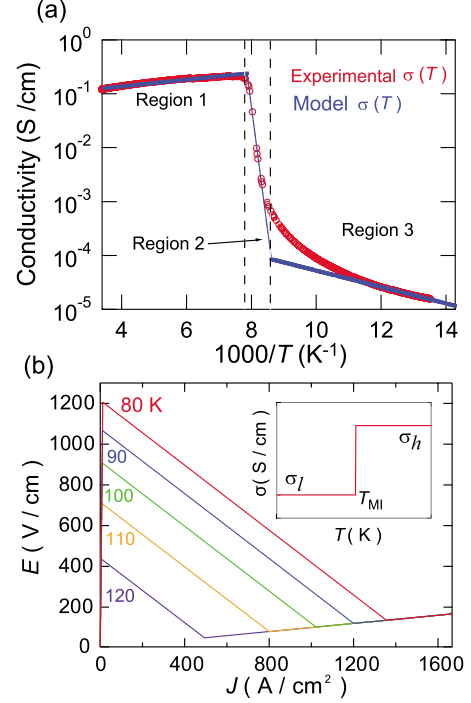

FIG. 3. (Color online) (a) Approximate temperature dependence of the conductivity for $\|b$ used in the simulation. (b) Simulated J-E characteristics in the 2P measurement based on the stepwise $\sigma(T)$ as shown in the inset.

these values jump to 3 Ω for $\|c$, the maximum current is limited by the load resistor (5 kΩ). Consequently, the ratio of the currents applied in the low-conducting and high-conducting states is less than 10, particularly for $\|c$, leading to the round peaks and small jumps. The resulting characteristics are similar to the 4P measurements. The triangular characteristics in the previous case are associated with the large current ratio more than 100. Since we cannot use too small load resistance in order not to destroy the sample, the round 2P characteristics in the present case is related to the comparatively small resistance at the high-conducting state.

B. Threshold

The threshold electric fields E_{th} extracted from the peaks in Figs. 2(a)–2(c) are plotted in Fig. 4(a). In all cases, E_{th} (solid lines) decreases with increasing temperature, in common with the previous activation type. The threshold current J_{th} (dashed lines), however, sometimes decreases and other times increases depending on the directions. Since J_{th} is the peak positions in Figs. 2(a)–2(c), this is obvious from the fact that the peaks move right or left depending on the directions. This contrasts with the activation type, where J_{th} always increases with increasing temperature. As shown in Fig. 4(b), the threshold power, which is a product of E_{th} and J_{th}, always decreases at high temperatures. In the activation type, this quantity always *increases* at high temperatures.[10] Accordingly, the transition type is most conveniently characterized by the decreasing threshold power.

In the simulation, both E_{th} and J_{th} decrease in all directions [Fig. 4(c)]. Consequently, the threshold power de-
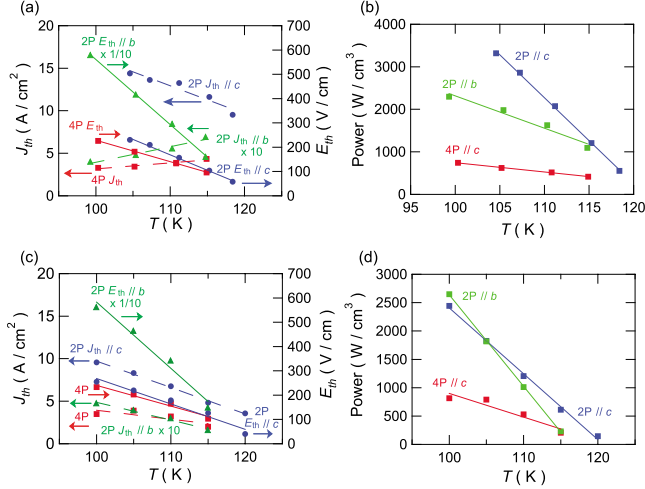
FIG. 4. (Color online) Temperature dependence of observed and simulated threshold currents, fields, and power in β''-(BEDT-TTF)$_3$(HSO$_4$)$_2$. (a) Observed temperature dependence of J_{th} and E_{th} extracted from Figs. 2(a)–2(c). Solid lines are for E_{th} and dashed lines for J_{th}. (b) Observed temperature dependence of the applied power $J_{th} \times E_{th}$ at the threshold, estimated from (a). (c) Simulated J_{th} and E_{th} extracted from Figs. 2(a)–2(c). Solid lines for E_{th} and dashed lines for J_{th}. (d) Simulated threshold power $J_{th} \times E_{th}$ estimated from (c).

creases [Fig. 4(d)]. In the activation type, we have naively neglected the K term in Eq. (3) leading to

$$P = nC\Delta T_e / \tau. \quad (4)$$

When ΔT_e is assumed to be constant, we obtain $E_{th} \propto \sigma^{-1/2}$ and $J_{th} \propto \sigma^{1/2}$, which account for decreasing E_{th} and increasing J_{th}. In the present transition type, the temperature dependence of the conductivity below T_{MI} is relatively small. If $\sigma(T)$ below T_{MI} is approximated to be constant, the jump to the high-conducting state occurs when T_e approaches to T_{MI}. By neglecting the C term in Eq. (3), this approximation affords,

$$E_{th} = \left(\frac{\alpha}{\sigma}\right)^{1/2}\sqrt{T_{MI} - T} \quad \text{and} \quad J_{th} = (\alpha\sigma)^{1/2}\sqrt{T_{MI} - T}, \quad (5)$$

where T is the temperature at the starting point. These equations indicate that both E_{th} and J_{th} decrease by increasing the starting T. In particular, the threshold power linearly decreases as $P = \alpha(T_{MI} - T)$. This linear dependence is fulfilled in Fig. 4(b). Since α is not only the material's intrinsic property but also depends on the sample dimensions, α may change depending on the directions. This is the reason why the slopes in Fig. 4(b) depend on the directions. In the simulation, different α is used for each direction. This naive approximation is exact when the resistivity is represented by a step function as shown in the inset in Fig. 3(b). In this extreme limit, $\sigma(T)$ jumps from the low-conducting state σ_l below T_{MI} to the high-conducting state σ_h above T_{MI}. The J-E characteristics are depicted in Fig. 3(b), where the low-conducting line, exactly represented by σ_l, jumps to the high conducting line, σ_h, at the threshold. This toy model explains why the threshold power decreases in the transition type.
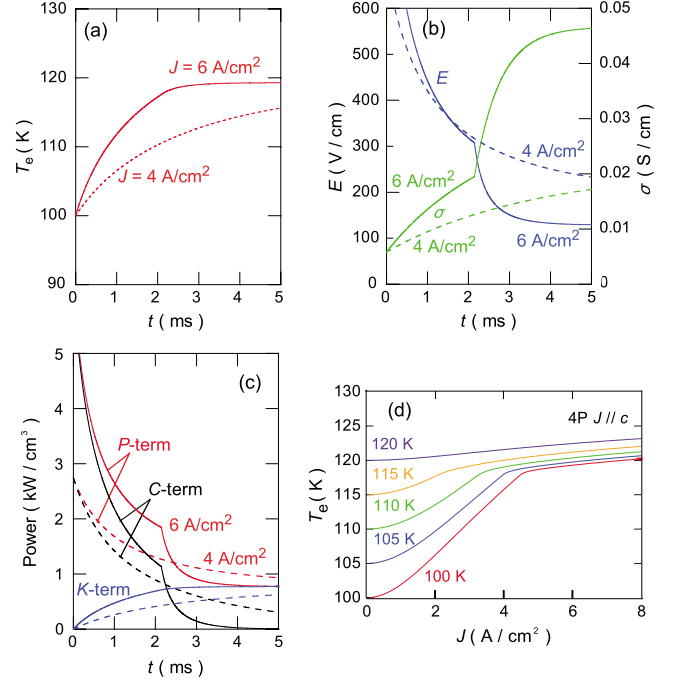

FIG. 5. (Color online) Transient behavior at $T = 100$ K in 4P$\|c$. (a) Time profiles of T_e, (b) E, σ, (c) P, K, and C terms in Eq. (3). The solid curves are for $J = 6$ A/cm^2 (above the threshold), and the dashed curves are for $J = 4$ A/cm^2 (below the threshold). (d) J dependence of T_e after 5 ms.

C. Transient states

Figures 5(a) and 5(b) show time profiles of T_e, E, and σ at $T = 100$ K in the 4P measurement. There appear two kinds of curves depending on the current; solid curves for $J = 6$ A/cm^2 show inflection points, whereas the dashed curves for $J = 4$ A/cm^2 are smooth. From Fig. 2(d), J_{th} is 4.4 A/cm^2 at this temperature. $J = 4$ A/cm^2 is below J_{th}, and the system remains in region 3 even at $t = 5$ ms, leading to the smooth curve. The $J = 6$ A/cm^2 curves above J_{th} enter region 2, resulting in inflection. At the same time, $\sigma(T)$ increases abruptly, and the P term in Eq. (3) drops [Fig. 5(c)], trapping T_e near the boundary between regions 2 and 3 [around 118 K from Fig. 5(a)]. After 5 ms, the P and K terms are equal [Fig. 5(c)], and the C term vanishes, realizing the steady state. The equilibrium T_e at various J is depicted in Fig. 5(d). The curves from 100 to 115 K have inflection points around $T_e = 118$ K, reflecting the border between regions 2 and 3. The inflection point of the 100 K curve appears at $J = 4.4$ A/cm^2, corresponding to the simulated J_{th}. Accordingly, the sharp NDR region just above J_{th} [Fig. 2(d)] is closely related to the sharp transition of $\sigma(T)$ at T_{MI} [Fig. 3(a)]. It should be recalled that the 4P measurement attains the steady state in the activation type.[10] As a consequence, the 4P characteristics are continuous everywhere. In the transition type, however, the characteristics have an inflection point depending on whether the final state remains in region 3 or enters the transition region (region 2).

Figure 6 shows time profiles at $T = 100$ K in the 2P measurement ($J\|c$). The threshold field is $E_{th} = 255$ V/cm from the peak top in Fig. 2(e) at this temperature, which corre-
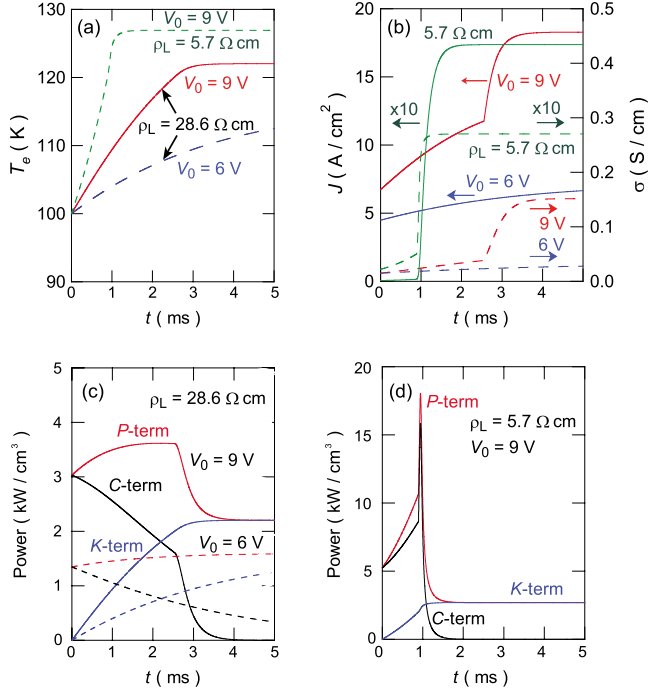
FIG. 6. (Color online) Transient behavior at 100 K in 2P∥c. (a) Time profiles of T_e; the solid curve is for V_0=9 V (above the threshold), and the dashed curve is for V_0=6 V (below the threshold). These curves are for ρ_L=28.6 Ω cm (R_L=5 kΩ), whereas the dotted curve is for ρ_L=5.7 Ω cm (R_L=1 kΩ) and V_0=9 V. (b) J and σ for these three cases. (c) P, K, and C terms in Eq. (3) for ρ_L=28.6 Ω cm. The solid curves are for V_0=9 V, and the dashed curves are for V_0=6 V. (d) P, K, and C terms in Eq. (3) for ρ_L =5.7 Ω cm and V_0=9 V.

sponds to V_0=7.4 V. The curves for V_0=9 V above E_{th} show inflection, whereas the curves for V_0=6 V are smooth similarly to the 4P measurements. It is obvious from Fig. 6(a) that the dashed curve for V_0=6 V does not enter region 2, and the equilibrium is not attained at 5 ms. When the load resistor is replaced from ρ_L=28.6 Ω cm (R_L=5 kΩ) to ρ_L =5.7 Ω cm (R_L=1 kΩ), the system reaches the high-conducting state within a shorter time [Fig. 6(a)]. The final T_e is trapped at T_{MI}=126 K, namely, at the border of regions 1 and 2. This contrasts with the 4P case, which is trapped at 118 K, because high resistance gives rise to high power. In contrast, the 2P case is trapped at the border to the low resistance state because the low resistance state gives rise to high power. As shown in Fig. 6(c), the P and K terms converge and the C term disappears in the steady state. Figure 6(d) for ρ_L=5.7 Ω cm demonstrates that the applied power has a sharp peak at the threshold when ρ_L is sufficiently small.

Figures 7(a) and 7(b) show the time profiles of V_s recorded on an oscilloscope at 106 K in the 2P measurements. In the previous activation type, the pulse consists of definite steps, and particularly the initial plateau is obvious.[9] In contrast, it is characteristic of the present case that the initial low-conducting region is inclined. As shown in Figs. 7(c) and 7(d), this inclination is reproduced by the simulation. This inclination is a direct result of the small current ratio of the low-conducting and high-conducting states. J and σ in
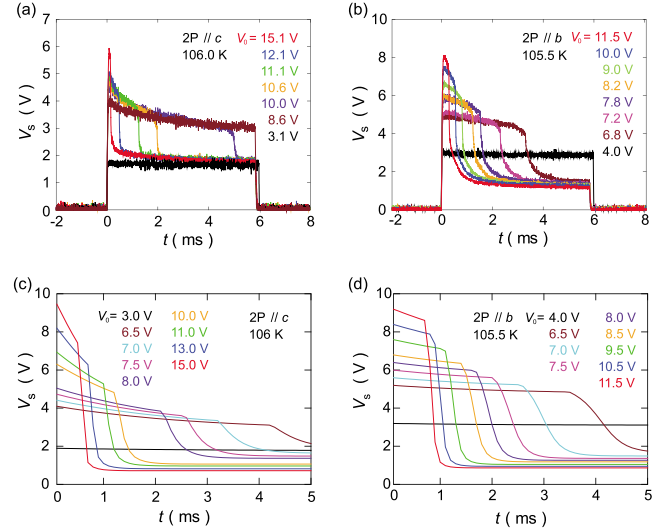

FIG. 7. (Color online) Pulse shape of V_s at 106 K for 2P. Observed pulses for (a) ∥c and (b) ∥b. Simulated time profiles for (c) ∥c and (d) ∥b.

Fig. 6(b) are the inverse of the output voltage. Accordingly, for large ρ_L=28.6 Ω cm (V_0=9 V) the current profile is inclined, while it becomes a sharp step for small ρ_L =5.7 Ω cm.

D. Nonlinear dynamics

In the above simulation, T_e has been calculated iteratively according to Eq. (3). In order to investigate how T_e changes successively, new $T_e+\Delta T_e$ calculated from Eq. (3) is plotted with respect to old T_e in Fig. 8(a). This is a plot called a return map in nonlinear dynamics.[18] The curves cross the slope=1 line at point A. Below point A, the curves are located above the slope=1 line, indicating that $T_e+\Delta T_e$ is higher than T_e. Consequently, T_e increases and approaches point A. Above point A, the curves are located below the slope=1 line, and T_e decreases to approach point A. Accordingly, point A is a stable point.

When artificially small nC=0.02 J/K cm³ is assumed, the point starting from B jumps above A, going to C, and oscillates between B and C. Then, period-2 oscillation appears. As shown in the bifurcation diagram in Fig. 8(b), the period-2 oscillation is stable up to very large $(nC)^{-1}$, and bifurcation to higher periodicity and chaos does not happen. This is because the local negative slope around A is much steeper than the global slope. The local negative slope becomes unstable while the global slope is stable, and only the period-2 oscillation is allowed to exist. Since the local steep slope is associated with the sharp phase transition, the absence of chaos is regarded as another token of the transition type.

V. CONCLUSION

The steep drops in 4P E-J characteristics in the present HSO₄ salt are explained in view of the sharp transition at T_{MI}. Although the characteristics are derived from the shape
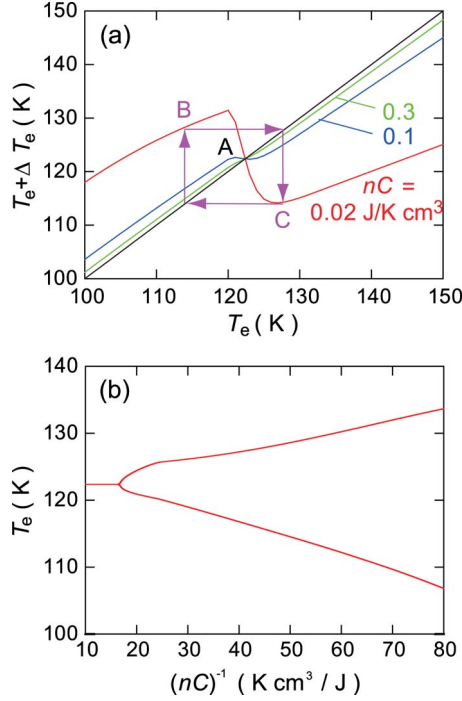
FIG. 8. (Color online) (a) Return map for 2P∥*c* at V_0=9.8 V, ρ_L=28.6 Ω cm, and *T*=100 K, where *nC* is decreased from 0.3 to 0.02 J/K cm³. (b) Bifurcation diagram at V_0=9.8 V and *T* =100 K.

of $\sigma(T)$, the same is expected to happen when the high electric fields and the resulting sufficient number of excited carriers destroy the energy gap. In contrast to this transition type, the activation type is realized when the energy gap is robust in any circumstances. In addition to the steep *E-J* characteristics, the negative temperature dependence of the threshold power and the absence of the chaotic outputs are characteristic of the transition type. The occurrence of chaos is associated with the continuous $\sigma(T)$ in the activation type.

The existence of a distinct phase transition above which the charge-order ground state disappears entirely seems to be a common case. Therefore, it is surprising that in most systems nonlinear conductivity has been interpreted by the power law, and the present transition type has not been recognized for a long time. There are several ways for the occurrence of charge order. In the quarter-filled systems such as θ phase, a stripe phase does not occur directly from the high-temperature uniform metallic phase,[19] and the intermediate non-stripe phase gives rise to complicated situations: a first-order transition between the different charge-order patterns or the glassy coexistence of the two patterns. In the present system, the direct transition from the uniform metal state to the charge order state is associated with the 3:2 composition, where the nonstripe charge order is the only possibility. This is the reason that the transition type has not been observed commonly.

The round peak and the small jump in the 2P *E-J* characteristics, as well as the inclined initial plateau in the pulse profile, are related to the considerably high-conducting nature of the present sample and the resulting small current ratio of the low-conducting and the high-conducting states.

In the present paper, we have discussed two categories as the extreme limits, but depending on the shape of $\sigma(T)$, the intermediate states may exist continuously. We will be able to discuss the intermediate states quantitatively starting from the present energy-balance model.

APPENDIX

Characteristics of inorganic transferred-electron devices have been most simply derived from a two-level model.[20] When carrier numbers in the ground and excited states are n_1 and n_2, respectively, the total current density is

$$J = e(n_1\mu_1 + n_2\mu_2)E, \tag{A1}$$

where μ_1 and μ_2 are the respective mobilities. The population difference is given by

$$\frac{n_2}{n_1} = R \exp\left(-\frac{T_a}{T_e}\right), \tag{A2}$$

where T_a is the energy difference between the two levels represented by *K* and *R* is the density-of-state ratio. Although n_2 increases not only by thermal excitation but also by high electric fields, this equation defines electron temperature, T_e. Inserting Eq. (A2) into Eq. (A1), we obtain

$$J = en_1\left[\mu_1 + \mu_2 R \exp\left(-\frac{T_a}{T_e}\right)\right]E. \tag{A3}$$

In the transferred-electron devices, the mobility at the excited state μ_2 is much smaller than μ_1, whereas now $\mu_2 \gg \mu_1$. In the steady state (dT_e/dt=0), Eq. (3) affords

$$\alpha(T_e - T) = JE. \tag{A4}$$

Equation (A3) is inserted in this equation to erase *E* leading to

$$\alpha(T_e - T) = \left\{en_1\left[\mu_1 + \mu_2 R \exp\left(-\frac{T_a}{T_e}\right)\right]\right\}^{-1} J^2. \tag{A5}$$

This equation self-consistently determines T_e under a given current. Putting the resulting T_e in Eq. (A4), we can obtain *E*, and the corresponding *J-E* characteristics. If we erase *J* from Eqs. (A3) and (A4), we obtain the characteristics under the constant voltage. However, the square bracket in Eq. (A5) is regarded as $\sigma(T_e)$, so that we go back to

$$\alpha(T_e - T) = J^2/\sigma(T_e). \tag{A6}$$

From this equation, we can estimate T_e in the steady state and obtain the *J-E* characteristics. Actually, if we assume $\sigma(T_e)$ as shown in Fig. 3(a), we attain the same curve as Fig. 2(c).

[1] G. Grüner, *Density Waves in Solids* (Addison-Wesley, Massachusetts, 1994).

[2] S. Cox, J. Singleton, R. McDonald, D. A. Migliori, and P. B. Littlewood, Nature Mater. **7**, 25 (2008).

[3] V. Markovich, I. Fita, A. I. Shames, R. Puzniak, E. Rozenberg, C. Martin, A. Wisniewski, Y. Yuzhelevskii, A. Wahl, and G. Gorodetsky, Phys. Rev. B **68**, 094428 (2003).

[4] K. Inagaki, I. Terasaki, H. Mori, and T. Mori, J. Phys. Soc. Jpn. **73**, 3364 (2004).

[5] T. Mori, H. Mori, and I. Terasaki, J. Mater. Chem. **17**, 4343 (2007).

[6] Y. Takahide, T. Konoike, K. Enomoto, M. Nishimura, T. Terashima, S. Uji, and H. M. Yamamoto, Phys. Rev. Lett. **96**, 136602 (2006).

[7] Y. Takahide, T. Konoike, K. Enomoto, M. Nishimura, T. Terashima, S. Uji, and H. M. Yamamoto, Phys. Rev. Lett. **98**, 116602 (2007).

[8] F. Sawano, I. Terasaki, H. Mori, T. Mori, M. Watanabe, N. Ikeda, Y. Nogami, and Y. Noda, Nature (London) **437**, 522 (2005).

[9] T. Mori, Y. Bando, T. Kawamoto, I. Terasaki, K. Takimiya, and T. Otsubo, Phys. Rev. Lett. **100**, 037001 (2008).

[10] T. Mori, T. Ozawa, Y. Bando, T. Kawamoto, S. Niizeki, H. Mori, and I. Terasaki, Phys. Rev. B **79**, 115108 (2009).

[11] D. M. Kroll, Phys. Rev. B **9**, 1669 (1974).

[12] Y. Iwasa, T. Koda, S. Koshihara, Y. Tokura, N. Iwasawa, and G. Saito, Phys. Rev. B **39**, 10441 (1989).

[13] L. C. Porter, H. H. Wang, M. M. Miller, and J. M. Williams, Acta Crystallogr. C **43**, 2201 (1987).

[14] N. D. Kush, V. N. Laukhin, A. I. Schegolev, E. B. Yagubskii, E. Yu. Alikberova and N. S. Rukk, J. Phys. I France, **1**, 1365 (1991).

[15] A. Miyazaki, T. Enoki, H. Uekusa, Y. Ohashi, and G. Saito, Phys. Rev. B **55**, 6847 (1997).

[16] T. Yamamoto, M. Uruichi, K. Yakushi, and A. Kawamoto, Phys. Rev. B **73**, 125116 (2006).

[17] J. M. Ziman, *Principles of the Theory of Solids*, 2nd ed. (Cambridge University Press, London, 1972).

[18] R. L. Devaney, *A First Course in Chaotic Dynamical Systems: Theory and Experiments* (Peseus, Massachusetts, 1992).

[19] T. Mori, J. Phys. Soc. Jpn. **72**, 1469 (2003).

[20] S. M. Sze, *Physics of Semiconductor Devices*, 2nd ed. (Wiley, New York, 1981), p. 645.